Aalto University

Aaltodoc

OPEN ACCESS

Author(s): Barbiellini, B. & Puska, M. J. & Korhonen, T. & Harju, A. & Torsti, T. & Nieminen, Risto M.

Title: Calculation of positron states and annihilation in solids: A density-gradient-correction scheme

Year: 1996

Version: Final published version

Calculation of positron states and annihilation in solids: A density-gradient-correction scheme

B. Barbiellini, M. J. Puska, T. Korhonen, A. Harju, T. Torsti, and R. M. Nieminen

Laboratory of Physics, Helsinki University of Technology, 02150 Espoo, Finland

The generalized gradient correction method for positron-electron correlation effects in solids [B. Barbiellini *et al.*, Phys. Rev. B **51**, 7341 (1995)] is applied in several test cases. The positron lifetime, energetics, and momentum distribution of the annihilating electron-positron pairs are considered. The comparison with experiments shows systematic improvement in the predictive power of the theory compared to the local-density approximation results for positron states and annihilation characteristics. [S0163-1829(96)03824-6]

I. INTRODUCTION

Experimental methods based on positron annihilation give valuable information on the electronic and ionic structures of condensed media, especially defects in solids.[1-3] The experimental output is, however, indirect, e.g., in the form of the lifetime of the positron or data related to the momentum content of the annihilating electron-positron pair in a specific environment. Clearly, the interpretation of these data calls for theoretical methods with quantitative predicting power.[4] On the other hand, the positron annihilation measurements give unique experimental data to be used in comparing the results of many-body theories for electron-electron and electron-positron interactions.

The modern *ab initio* electronic-structure calculations for the properties of different types of materials including perfect crystal lattices, defect and surface systems, and finite clusters of atoms are usually based on the density-functional theory (DFT).[5] The success of the DFT stems from the fact that the electron-electron interactions can be handled simply, but with often sufficient accuracy using the local-density approximation (LDA) for the exchange and correlation effects.

The calculation of positron states and annihilation characteristics can also be based on the DFT. For delocalized positron states in perfect lattices the usual DFT for an electronic system is the sufficient starting point, because the locally vanishing positron density does not affect the electronic structure. The DFT calculations for positron states usually employ the LDA. This means that for the effective positron potential the attractive part due to the electron-positron correlation effects is obtained from the local electron density and using the results of the many-body calulations for a delocalized positron in a homogeneous electron gas. The LDA also means that the results of these many-body calculations are used also for the contact electron density at the positron site that determines the positron annihilation rate.

In the case of a positron trapped by a defect the maximum of the positron density may be of the same order as the local electron density. Then one should base the calculations on the two-component density functional theory (TCDFT),[6] which solves for the mutually self-consistent electron and positron densities. However, practical calculations[6,7] have shown that due to canceling effects, the "conventional" scheme, in which the electron density is calculated without

the effect of the localized positron, gives results very similar to the full two-component calculations. The conventional scheme can be justified by stating that the positron with its screening cloud forms a neutral quasiparticle that does not affect the remaining electronic system, i.e., the total electron density of the system is a superposition of the "clean" system density and the positron-induced screening cloud. We will adopt the conventional scheme in this paper also when calculating positron states at vacancy defects.

The shortcomings of the LDA in the electronic-structure calculations are well known. They include too diffuse electron densities of atoms, the overbinding in molecules and in solids, and the too narrow band gaps of semiconductors and insulators.[5] Therefore, it is not surprising that the LDA for positron calculations also has problems.[8] First, the LDA electron-positron correlation potential fails clearly for positrons outside solid surfaces and in insulators such as rare-gas solids, in which cases the screening electron cloud cannot follow the positron. To remedy this deficiency one has to employ a nonlocal construction such as the weighted density approximation[9] or use some *ad hoc* approach.[10] Second, when calculating the positron annihilation characteristics for solids the LDA has shown a clear tendency to overestimate the rate of positron annihilation. One has tried to correct this deficiency by omitting the electron-positron correlation (enhancement) when calculating the annihilation with core electrons.[11,12] In the case of semiconductors one can argue that the positron screening by valence electrons is, due to the band gap, weaker than in an electron gas. This idea has been successfully used in a semiempirical approach, which accounts for the reduced screening ability by using the (finite) high-frequency dielectric constant as a parameter. The two-dimensional angular correlation of the annihilation radiation (2D ACAR) measurements for several transition metals[3,13] indicate that the enhancement for *d* electrons is smaller than predicted by the LDA calculations. Finally, it has been pointed out that the more accurate the many-body calculation for the homogeneous gas, the higher the annihilation rate increasing the discrepancy between the theoretical and experimental positron lifetimes.[14]

In the electronic-structure calculations, several attempts and suggestions to go beyond the LDA have been studied.[5,15] Over the past years especially the generalized gradient approximation (GGA) has attracted wide interest.[16] In the GGA

the gradient of the electron density is included, in addition to the local density. The GGA is able to improve the description of some of the cohesive properties compared to the LDA,[17] but a general improvement in different kinds of systems has not yet resulted (see, for Ref. 18). An example of a physical situation in which the use of the GGA for the electronic-structure calculation provides a significant improvement over the LDA is the H_2 dissociation on the Cu(111) surface.[19] It has also been showed that the GGA gives results in better agreement with the experiments than the LDA for finite systems (atoms and molecules) and for metallic surfaces.[20,21] One reason is that the interactions in these systems are related to the tails of the electronic wave functions, for which the GGA should, in principle, give a better description than the LDA.

Recently, we have proposed a GGA method for positron states in solids.[22] Clearly, the screening of the positron should depend not only on the local electron density but also on its gradient as well. In the case of positrons, the GGA should be done consistently for both the electron-positron correlation potential and the contact electron density at the positron. The latter is an aspect which is not met in the pure electronic-structure calculations. Because the contact density can be directly monitored by different types of positron annihilation measurements, the comparison of the theoretical and experimental positron annihilation parameters is a unique method for testing many-body theories such as DFT and different approximations within them. In order to use consistent data for the electron-positron correlation energy and the contact density, we introduce for the latter an interpolation form based on the many-body calculations of Arponen and Pajanne.[23]

The results obtained for the properties of solids using the GGA for the electronic structure show some scatter.[24,25] This is presumably a result of computational approximations such as the pseudopotential approximation or the shape approximations for the electron density or potential. In the case of GGA for positron states we therefore study different methods for constructing the electron density. The methods include the linear muffin-tin orbital (LMTO) method within the atomic-spheres approximation[26] (ASA) and the atomic superposition method.[27] In the LMTO ASA method the electron density and the potentials are self-consistent, but they are assumed to be spherical. In the atomic superposition method there are no shape approximations, but the electronic structure is non-self-consistent. Moreover, we compare several calculated annihilation parameters, i.e., the positron lifetime, positron affinity, and the 2D ACAR maps, with their experimental counterparts. The comparison of the theoretical and experimental results is easiest in the case of perfect crystal lattices, which have delocalized positron states. However, we also consider localized positron states trapped at vacancies of the crystal lattice.

II. THEORY

The determination of electron and positron states in solids is possible on the basis of the TCDFT.[6] In the conventional scheme, which is exact for delocalized positron states, the electron density $n^-(\mathbf{r})$ is first calculated without the effect of the positron. In the Kohn-Sham method the electron density

is obtained from the single-electron wave functions $\psi_i^-(\mathbf{r})$

$$n^-(\mathbf{r}) = \sum_i |\psi_i^-(\mathbf{r})|^2, \qquad (1)$$

where the sum is over the occupied states i. Then the effective potential $V^+(\mathbf{r})$ for a positron is constructed as the sum of Coulomb $V_{\text{Coul}}(\mathbf{r})$ and electron-positron correlation parts $V_{\text{corr}}(\mathbf{r})$

$$V^+(\mathbf{r}) = V_{\text{Coul}}(\mathbf{r}) + V_{\text{corr}}(\mathbf{r}). \qquad (2)$$

The Coulomb part arises from the nuclei and from the Hartree potential of the electron density $n^-(\mathbf{r})$. The correlation part describes the energy lowering due to the pileup of the screening charge around the positron. In the LDA for the positron states $V_{\text{corr}}(\mathbf{r})$ for a given point is calculated from the electron density at that point. That is,

$$V_{\text{corr}}^{\text{LDA}}(\mathbf{r}) = \epsilon_{\text{corr}}^{\text{EG}}[n^-(\mathbf{r})], \qquad (3)$$

where $\epsilon_{\text{corr}}^{\text{EG}}(n^-)$ is the electron-positron correlation energy per a delocalized positron in a homogeneous electron gas with density n^-. After the positron potential is constructed its wave function $\psi^+(\mathbf{r})$ and energy eigenvalue are solved from the corresponding one-particle Schrödinger equation.

In the DFT the Kohn-Sham wave functions are actually auxiliary functions used to construct the total density, which is the quantity with a real physical meaning in the theory. The wave functions are, however, customarily used as real single-particle wave functions in many different contexts.[5] In this work we will also start the discussion of the positron annihilation characteristics by using the single-particle wave functions for electrons and we will actually employ the Kohn-Sham wave functions in calculating the momentum distribution of the annihilating electron-positron pairs.

The positron annihilation rate as a function of the momentum $\mathbf{p}$ of the annihilating positron-electron pair is determined from the electron and positron wave functions as[28,4]

$$\rho(\mathbf{p}) = \pi r_e^2 c \sum_i \left| \int e^{i\mathbf{p}\cdot\mathbf{r}} \psi^+(\mathbf{r}) \psi_i^-(\mathbf{r}) \sqrt{\gamma_i(\mathbf{r})} d\mathbf{r} \right|^2, \qquad (4)$$

where r_e is the classical electron radius and c is the speed of light. The summation is over all occupied electron states. $\gamma_i(\mathbf{r})$ is the enhancement factor for the ith state, i.e., the ratio between the contact electron density at the positron and unperturbed (host) electron density at that point.

The shape of ACAR spectra of the s and p valence electrons in simple metals is already well described by a constant state-independent enhancement factor, i.e., within the independent particle model (IPM) in which $\gamma_i(\mathbf{r}) \equiv 1$.[3] Kahana[29] has applied the Bethe-Golstone formalism to a positron in the homogeneous electron gas and found that the enhancement factor has a momentum dependence. Kahana proposed the parametrization[29]

$$\gamma_i = \epsilon(p) = a(r_s) + b(r_s)(p/p_f)^2 + c(r_s)(p/p_f)^4, \quad p \lesssim p_F, \qquad (5)$$

where r_s is the electron density parameter $[r_s = (3/4\pi n_-)^{1/3}]$ and p_F is the Fermi momentum (in atomic units $p_F = 1.92/r_s$). The 2D ACAR measurements

performed for the alkali metals have yielded experimental values for the ratios b/a (0.0 for Li and Na, 0.2 for K) and c/a (0.2 for Li, 0.4 for Na and K).[31] In inhomogenous systems the position dependence of $\gamma_i(\mathbf{r})$ is much more important than the state dependence. In that case the enhancement factor $\gamma_i(\mathbf{r})$ in the momentum density equation (4) can be approximated by the average over the states i, $\gamma(\mathbf{r}) = \langle \gamma_i(\mathbf{r}) \rangle$.[32] In this approximation the effect of the enhancement factor to the momentum content is similar to that of including the positron wave function.

The total annihilation rate is obtained from Eq. (4) by integrating over the momentum. The result is

$$\lambda = \pi r_e^2 c \int n^+(\mathbf{r}) n^-(\mathbf{r}) \gamma(\mathbf{r}) d\mathbf{r}. \qquad (6)$$

The positron lifetime τ is then the inverse of the annihilation rate λ. Equation (6) is in the spirit of the DFT in the sense that the total densities, not the wave functions, are involved. In the LDA for the positron states the enhancement factor $\gamma(\mathbf{r})$ is calculated as

$$\gamma^{\mathrm{LDA}}(\mathbf{r}) = \gamma^{\mathrm{EG}}[n^-(\mathbf{r})], \qquad (7)$$

where $\gamma^{\mathrm{EG}}(n^-)$ is the enhancement factor for the homogeneous electron gas. Our aim in this work is to go beyond the LDA by introducing into Eqs. (7) and (3) corrections depending on the gradient of the electron density. However, first we consider in Sec. II A the electron-positron correlation in the homogeneous electron gas.

The 2D ACAR experiments do not give directly the momentum distribution of Eq. (4) but its integral along a certain direction[3]

$$N(p_x, p_y) = \int \rho(\mathbf{p}) dp_z. \qquad (8)$$

Actually the experimental information is the integral $N(p_x, p_y)$ convoluted by the experimental resolution function. The Lock-Crisp-West (LCW) folding of the 2D ACAR data allows one to put in evidence the Fermi surface breaks by giving the partial positron annihilation rates for occupied electronic states at given $\mathbf{k}$ points within the first Brillouin zone. The LCW folding of the momentum distribution of Eq. (4) is defined as

$$\lambda(\mathbf{k}) = \mathrm{const} \sum_{\mathbf{G}} \rho(\mathbf{k} + \mathbf{G}) = \pi r_e^2 c \int n^+(\mathbf{r}) n^-(\mathbf{r},\mathbf{k}) \gamma(\mathbf{r}) d\mathbf{r}, \qquad (9)$$

where $\mathbf{G}$ is a reciprocal lattice vector and $n^-(\mathbf{r},\mathbf{k})$ is the density of the occupied electronic states at $\mathbf{k}$. If the positron density n^+ and the enhancement factor γ are constants, one obtains the electron momentum distribution in the first Brillouin zone (the Lock-Crisp-West theorem[33]). In the case of metals, this distribution consists of occupied valence-state regions with a certain constant density separated by the so-called Fermi-surface breaks from the unoccupied valence-state regions with a lower density. According to the measurements, however, $\lambda(\mathbf{k})$ varies for different $\mathbf{k}$ and thus the Fermi-surface breaks are modulated by the positron wave function and the enhancement effects. As the unfolded 2D ACAR data, also its LCW folding is actually an integral of
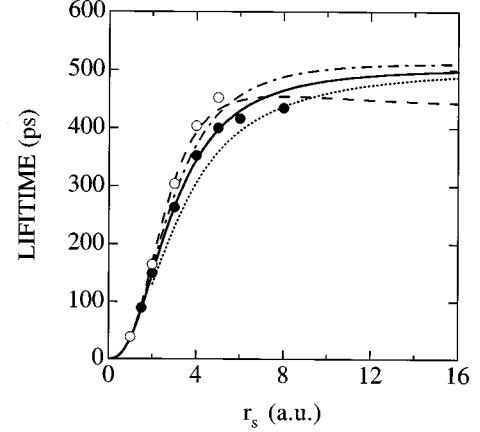

FIG. 1. Positron lifetime in a homogeneous electron gas as a function of the density parameter r_s. The results of the many-body calculations by Arponen and Pajanne (Ref. 23) and those by Lantto (Ref. 34) are shown as filled and open circles, respectively. The lifetimes obtained in the scaled proton approximation (Ref. 37) are denoted by a dotted line. The Stachowiak-Lach (Ref. 14) result is drawn by a dash-dotted line. The interpolation function by Boroński and Nieminen (Ref. 6) and the present one [Eq. (10)] are drawn by a dashed and by a solid line, respectively.

the momentum distribution along a certain direction. This fact reduces the detailed information content of the data.

A. Positron in a homogeneous electron gas

The DFT LDA calculations for positron states in solids are based on many-body calculations for a delocalized positron in a homogeneous electron gas. Several approaches exist for solving this model system. The scheme of Arponen and Pajanne[23] is based on correcting the results of the random-phase approximation (RPA) in a boson formalism. Lantto[34] has used the hypernetted-chain approximation. The calculations by Arponen and Pajanne are generally considered as the most accurate ones.[34,14] The situation is, however, much less satisfactory than in the case of the clean homogeneous electron gas for which accurate Monte Carlo calculations exists.[35] The difficulty in the Monte Carlo calculations for a positron in a homogeneous electron gas arise from the fact that very high statistics are needed for an accurate description of the electron cusp at the positron.[36]

For the correlation energy, Boroński and Nieminen[6] have given an interpolation form, which for the metallic densities follows the data calculated by Arponen and Pajanne. We will adopt this interpolation form for the present calculations. In the case of the enhancement factor the situation is not so straightforward. Figure 1 shows the ensuing positron lifetime in a homogeneous electron gas as a function of the density parameter r_s. The results of the many-body calculations by Arponen and Pajanne[23] as well as those by Lantto[34] are shown as discrete points. Figure 1 shows also the result of the theory by Stachowiak and Lach.[14] The lifetimes estimated by scaling[37] the contact density for a proton in a homogeneous electron gas are added. They give a rigorous lower bound for the positron lifetime. At low densities all the results approach the value of 500 ps, which is the average lifetime for a positronium atom. The scatter in the results of

the many-body calculations is surprisingly large. In the region, important for the transition metals, i.e., slightly above 100 ps, the scatter is about 15 ps. Around 230 ps, which is typical for semiconductors, the scatter is close to 30 ps.

The widely used function by Boroński and Nieminen[6] interpolating Lantto's results is also shown in Fig. 1. It reproduces quite faithfully Lantto's points, but at low electron densities it gives unphysically low lifetimes. We are not satisfied with this parametrization and for the practical calculations we have made another interpolation function. We use the results by Arponen and Pajanne[23] because we want the lifetime calculations to be consistent with the correlation energy used. Our enhancement function reads as

$$\gamma = 1 + 1.23 r_s - 0.0742 r_s^2 + \tfrac{1}{6} r_s^3. \tag{10}$$

This function has the same form as that used by Stachowiak and Lach.[14] As a matter of fact, the only fitting parameter in this equation is the factor in the front of the square term. The first two terms are fixed to reproduce the high-density RPA limit and the last term the low-density positronium limit. In the fitting procedure we have used the Arponen-Pajanne data points only up to $r_s = 5$ because the data at lower densities is less reliable [the Friedel sum rule is not obeyed for $r_s = 6$ and 8 (Ref. 23) and the $r_s = 8$ point reaches even the scaled proton limit in Fig. 1]. As we will see below, the positron lifetimes calculated in the LDA with this interpolation formula are systematically lower than the experimental ones.

B. Positron in an inhomogeneous electron gas

1. Gradient correction for the positron annihilation rate

The LDA shows in electronic-structure calculations a clear tendency to overestimate the magnitude of the correlation energy. This is seen, for example, in the case of free atoms, for which comparison with experiments is possible.[38] The overestimation of the correlation energy has been traced back to the shape of the correlation hole close to the electron. In the GGA for electrons the correlation energy is improved by reducing the charge redistributed by the correlation hole near the fixed electron (for a definition of this redistributed charge, see Ref. 39). Similarly, the gradient correction for the electron-positron correlation should reduce the electron density near the positron and thereby decrease the enhancement factor and increase the positron lifetime. This will also reduce the magnitude of the electron-positron correlation energy.

In the GGA the effects of the nonuniform electron density are described in terms of the ratio between the local length scale $n/|\nabla n|$ of the density variations and the local Thomas-Fermi screening length $(q_{TF})^{-1}$ [in atomic units $q_{TF} = \sqrt{(4/\pi)} p_F$]. The lowest-order gradient correction to the LDA correlation hole density is proportional to the parameter[38]

$$\epsilon = |\nabla n|^2/(n q_{TF})^2 = |\nabla \ln n|^2/q_{TF}^2. \tag{11}$$

We use this parameter in describing the reduction of the screening cloud close to the positron. In the case of a uniform electron gas $\epsilon = 0$, whereas when the density variations are rapid ϵ approaches infinity. At the former limit the LDA result for the induced screening charge is maintained and the

latter limit leads to the IPM result with no enhancement. We interpolate between these limits by using for the induced contact screening charge Δn the form

$$\Delta n_{GGA} = \Delta n_{LDA} \exp(-\alpha \epsilon). \tag{12}$$

The corresponding enhancement factor reads

$$\gamma_{GGA} = 1 + (\gamma_{LDA} - 1)\exp(-\alpha \epsilon). \tag{13}$$

Above, α is an adjustable parameter. It will be determined so that the calculated and experimental lifetimes agree as well as possible for a large number of different types of solids. We have found that the $\alpha = 0.22$ used with the interpolation form of Eq. (10) gives lifetimes for different types of metals and semiconductors, in good agreement with experiment.

In our previous work[22] we showed that the GGA strongly reduces the enhancement factor in the ion core region. The resulting enhancement factor reflects sensitively the shell structure of the atom in question in the sense that it is nearly constant over the spatial region dominated by a given shell. This means that the old scheme,[40,27] in which the annihilations with different atomic shells are separated and constant enhancement factors are used for the d and core shells, finds partial justification within the DFT, i.e., using the total electron density as the starting point.

The present GGA model for positrons reduces the contact density at the positron. This means that the screening decreases, approaching zero at the IPM limit of $\epsilon \to \infty$. In this sense the GGA model is related to the model by Puska *et al.*[41] for positron annihilation in semiconductors. In that model the contact density decreases because the normalization of the screening cloud is changed to correspond to the reduced screening in semiconductors relative to the perfect screening in a free-electron-gas model relevant for metals. In the semiconductor model by Puska *et al.* the norm of the screening cloud depends on the high-frequency dielectric constant of the material. Puska *et al.* showed that the model used with the Boroński-Nieminen interpolation scheme gives positron lifetimes for group-IV and III-V semiconductors in good agreement with experiments and that experimental variations seen in the positron lifetime can be correlated with the variations in the high-frequency dielectric constant.

2. Gradient correction for the electron-positron correlation potential

Let us suppose that the electron-positron correlation for an electron gas with a relevant density is mainly characterized by one length a, as is the case of the scaled positronium approximation.[9] Then for the electron-positron correlation energy $dE^{corr}/d(1/a)$ is constant and the normalization factor of the screening cloud scales as a^d with $d = 3$ for the dimension of space. Compared to the IPM result, the electron-positron correlation increases the annihilation rate as $\lambda - \lambda_{IPM} = (\gamma - 1)\lambda_{IPM}$, which is proportional to the density of the screening cloud at the positron. Consequently, we have the scaling law[42]

$$E^{corr} = c_1 (\lambda - \lambda_{IPM})^{1/d} + c_2. \tag{14}$$

In the scaled positronium approximation, the second coefficient $c_2 = 0$ and the correlation energy in rydbergs reads as

$$E^{\text{corr}} = -\frac{[3/4(\gamma-1)]^{1/3}}{r_s}. \tag{15}$$

The values of the correlation energy calculated by Arponen and Pajanne[23] obey the form of Eq. (15) quite well and the coefficient c_2 has a relatively small value of 0.11 Ry. Therefore, one can use in the practical GGA calculations the correlation energy $E^{\text{corr}}_{\text{GGA}}$, which is obtained from the homogeneous-electron-gas result ($E^{\text{corr}}_{\text{LDA}}$) by the scaling

$$E^{\text{corr}}_{\text{GGA}}(\mathbf{r}) = E^{\text{corr}}_{\text{LDA}}[n_-(\mathbf{r})]\left(\frac{\lambda_{\text{GGA}}-\lambda_{\text{IPM}}}{\lambda_{\text{LDA}}-\lambda_{\text{IPM}}}\right)^{1/3}$$

$$= E^{\text{corr}}_{\text{LDA}}[n_-(\mathbf{r})]e^{-\alpha\epsilon/3}, \tag{16}$$

where λ_{LDA} and λ_{GGA} are the annihilation rates in a homogeneous electron gas, i.e., in the LDA model, and in the GGA model, respectively. We use for the correlation energy $E^{\text{corr}}_{\text{LDA}}$ the interpolation form of Ref. 6. Our formula (16) neglects the small term $c_2(1-e^{-\alpha\epsilon/3})$. Moreover, with the rescaling of the potential we are not able to describe the image potential at a metallic surface seen by the positron.[9]

The resulting positron potential is more repulsive in the GGA than in the LDA. The open volume for the positron state decreases in the GGA, raising the positron zero-point energy. This effect can be seen in the calculated positron affinities A_+. The affinity is defined as[43]

$$A_+ = \mu_- + \mu_+, \tag{17}$$

where μ_- and μ_+ are the electron and positron chemical potentials measured with respect to a common electrostatic crystal zero, i.e., μ_- and μ_+ are the position of the Fermi level and the bottom of the lowest positron band, respectively. The positron affinity can be measured using the slow positron beam techniques.[44,45] The comparison of the theoretical and experimental positron affinities directly tests the validity of the positron potential construction.

III. RESULTS AND DISCUSSION

In order to test the GGA scheme we perform calculations for positron states and annihilation characteristics for perfect crystal lattices as well as for lattices containing vacancies. We use the LMTO method within the ASA (Ref. 26) and the atomic superposition method.[27] In the LMTO ASA the self-consistent potentials and charge densities are spherical around the nuclei and in the case of diamond-type lattices also around interstitial tetrahedral sites. In the atomic superposition method the electron density and the Coulomb potential are constructed non-self-consistently by overlapping free atom densities and Coulomb potentials, respectively. The full three-dimensional geometry of the problem is retained and the resulting three-dimensional Schrödinger equation is solved in a real-space point mesh.[27,30] We calculate the momentum distribution (4) with the scheme by Singh and Jarlborg[46] using the LMTO ASA method and including the corrections for the effects of the overlapping spheres. Vacancy calculations are performed with the LMTO ASA or the atomic superposition method within the supercell approximation. Periodic boundary conditions have been employed for the positron state (positron wave vector $\mathbf{k}\equiv\mathbf{0}$). In

the LMTO ASA calculations we use a basis set consisting of s partial waves for delocalized positron states, whereas for states at vacancies we enlarge the basis by including also p and d waves. The lattice constants used in the calculations are the experimental ones for the very low temperatures. The lattice constant used are quoted in Refs. 43 and 41.

A. Positron lifetimes and affinities in perfect crystal lattices

The positron lifetimes and affinities calculated for several types of perfect solids in the LDA and GGA models are compared in Table I. The GGA increases the positron lifetime relative to the LDA both according to the LMTO ASA and the atomic superposition method. This is mainly due to the change in the enhancement factor; the differences in the correlation potentials influence through the changes in positron wave function, but this effect is small. Among the elemental materials the increase of the positron lifetime is largest, about 20%, for the alkali metals (except Li), late transition metals, and noble metals. Similar increases are seen also for elemental solids (Zn and Ge) and compounds (III-V and II-IV compounds) with relatively high-lying filled d bands. The common feature for these materials is the relatively high annihilation rate with core electrons (including the uppermost d electrons). The GGA suppresses very efficiently the enhancement factor for the core and d-band electrons. For the earth-alkali and the early transition metals the increase of lifetime due to GGA is smaller, around 10%, and for the Al with a very compact core electron structure the increase is only about 5%.

A set of the calculated LDA and GGA positron lifetimes of Table I are compared with experimental values in Fig. 2. We have tried to make a collection that represents many types of solids, but, on the other hand, we have tried to use as few experimental sources as possible. This is because we want to get reliable trends between different materials also when the lifetime differences are small. The LDA results are consistently below the experimental positron lifetimes. However, it is interesting to note that the LDA results fall quite accurately on the same line and that good agreement with experiment can be achieved simply by multiplying the LDA results by a constant. A least-squares fit with the theoretical values corresponding to the enhancement factor of Eq. (10) gives the value of 1.21 for this constant. A similar behavior is valid also for the LDA results obtained using the Boronski-Nieminen enhancement form,[6] but the constant factor is somewhat smaller, about 1.1. With the exception of Al, the GGA results agree well with the experiment, showing that the GGA is able to introduce a correction that is proportional to the calculated positron lifetime itself. For the materials in Fig. 2 (with the striking exception of Al) the GGA corrections to the LDA are quite similar, about 20 %. Therefore the good agreement seen in Fig. 2 may be to some extent fortuitous. In order to see if the finer details of GGA are also physical, it would be very interesting to compare experimental and GGA lifetimes for the early transition metals for which the relative GGA corrections are clearly smaller. Unfortunately, it is hard to find a consistent and comprehensive set of experimental lifetimes for transition metals.

Positron lifetimes calculated for several materials using the atomic superposition method are given in Table I. The

TABLE I. Theoretical positron bulk lifetimes τ for different types of solids. The results are obtained with the LMTO ASA or the atomic superposition method using the LDA enhancement factor of Eq. (2) and the corresponding GGA with $\alpha = 0.22$. In the atomic superposition method the ground-state electronic configurations are used for the free atoms. For example, the configuration $3d^{10}4s$ is used for Cu, whereas the results obtained with the configuration $3d^9 4s^2$ are given within parenthesis for comparison.

Material	Lattice	LMTO ASA τ^{LDA} (ps)	τ^{GGA} (ps)	Atomic superposition τ^{LDA} (ps)	τ^{GGA} (ps)
Li	bcc	257	282	259	284
C	diamond	86	96	84	93
Na	bcc	279	329	281	337
Al	fcc	144	153	149	160
Si	diamond	186	210	184	207
K	bcc	329	392	332	402
Ca	fcc	245	276	250	281
Sc	fcc	167	189	173	198
Ti	fcc	127	145	132	153
V	bcc	103	119	107	125
Cr	bcc	91	105	96	118
Mn	fcc	93	108	97	114
Fe	bcc	91	108	94	111
Co	fcc	89	106	91	109
Ni	fcc	88	107	90	109
Cu	fcc	96	118	101(98)	130(120)
Zn	fcc	120	144	124	156
Ge	diamond	191	228	190	229
Rb	bcc	341	409	343	420
Nb	bcc	109	122	114	135
Mo	bcc	101	112	106	126
Pd	fcc	94	114	99	131
Ag	fcc	109	136	113	148
Cs	bcc	356	430	358	439
Ta	bcc	108	117	108	124
W	bcc	93	101	95	109
Pt	fcc	88	101	92	116
Au	fcc	98	118	102	130
SiC	zinc blende	124	139	121	134
GaAs	zinc blende	190	231	190	232
InP	zinc blende	201	248	200	247
ZnS	zinc blende	179	223	179	232
CdTe	zinc blende	228	290	228	310
HgTe	zinc blende	222	285	222	310
TiC	rocksalt	94	110	101	116
$YBa_2Cu_3O_7$		120	157	143	188

LDA results for the bcc and fcc metals are typically less than 5 ps longer than those obtained by the LMTO ASA method. In the case of the diamond and zinc-blende structures the atomic superposition gives slightly, of the order of 2 ps, shorter lifetimes than or very similar lifetimes to the LMTO ASA method. In the LDA there exists an efficient feedback effect, which tries to keep the positron lifetime unchanged irrespective of the small transfers of electron density.[27,7] In the present comparison the electron density changes from the non-self-consistent superposition of free atom densities to
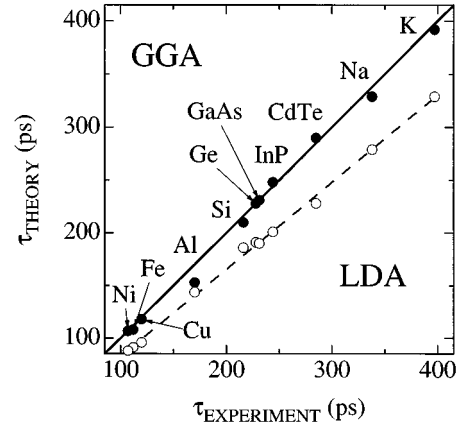

FIG. 2. Positron lifetimes in perfect lattices. The solid and open circles give the GGA and LDA results as a function of the experimental ones (Ref. 48), respectively. The solid line corresponds to the perfect agreement between the theoretical and experimental results, whereas the dashed line is a linear least-squares fit to the LDA data.

the self-consistent density of the solid. The positron density is calculated in each case according to the electron density in question. Thereby the positron density follows the transfer of the electron density in such a way that the overlap and the positron lifetime change only slightly. The shape approximation (spherical charge distributions and potentials) made in the LMTO ASA can partly be considered as such a charge transfer and its effect the positron lifetime is also quite small.

In contrast with the LDA, the positron lifetimes obtained in the GGA using the atomic superposition method differ in some cases quite strongly from their LMTO ASA counterparts. The reason is that the gradient is sensitive to the self-consistency and the shape of the electron density. This is seen clearly in the case of Cu for which we have used two different atomic configurations, $3d^{10}4s$ and $3d^9 4s^2$ (see Table I). The latter configuration gives in the GGA a lifetime close to the LMTO ASA value. When the configuration is changed to $3d^{10}4s$ the positron lifetime increases by 10 ps. For comparison, in the LDA the difference is only 3 ps due to the feedback effect. In the case of II-VI compound semiconductors the strong charge transfer between the atoms is not taken properly into account in the atomic superposition calculations. This is also seen to affect remarkably the positron lifetimes calculated within the GGA. The shape approximation of the ASA is not expected to influence the comparison of the GGA results between the LMTO ASA and the atomic superposition method, because the GGA correction arises mainly in the ion core region where the true electron density is spherical. Therefore, one can conclude that in order to get accurate positron lifetimes in the GGA, self-consistent electron densities should be used. However, it could be possible to improve the atomic superposition results by using for free atoms electronic configurations that correspond to the partial-wave expansions of the LMTO ASA method.[47]

The GGA reduces the percentages of the core electron contributions relative to the total annihilation rates. In the case of the alkali metals (with the exception of Li) the core
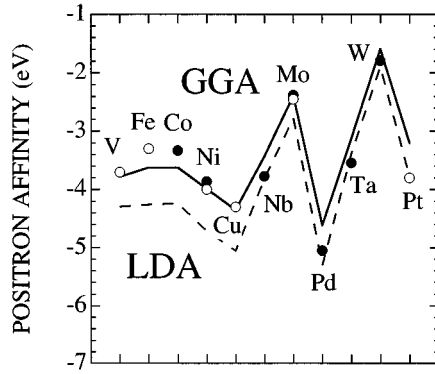
FIG. 3. Positron affinities in perfect lattices. The solid and dashed lines are drawn through the GGA and LDA results, respectively. The open and filled circles are the experimental results by Jibaly *et al.* (Ref. 44) and by Gidley and Frieze (Ref. 45).

contributions are large, about 25–35 % in the LDA, as in the calculation by Daniuk *et al.*[47] The GGA reduces them by about one-third. For Al and Ca, the core contributions are 9.3% and 23.0% in the LDA, respectively, and 5.9% and 16.3% in the GGA, respectively. In the case of semiconductors, the relative core contributions are small in magnitude, e.g., 3.1% for Si and 11.0% for GaAs in the LDA. This reflects the large interstitial open volume. The reduction due to the GGA is typically smaller for semiconductors than for metals. The values for Si and GaAs are 2.3% and 9.3% in the GGA, respectively. The relative core contribution can be estimated from the ACAR or from the coincidence Doppler line-shape data. An accurate estimation may, however, be difficult due to superposition of the core and the umklapp components of the valence annihilation at high momentum values. On the other hand, in the theory an unambiguous distinction between the core and valence electrons is difficult. For instance, in the case of the transition, noble, and Zn-column metals, as well as the II-VI compound semiconductors, the uppermost d electrons have to be treated as band states, which can hybridize with the s valence states.

The positron affinities calculated within the LDA and GGA models are compared with those measured by the re-emitted positron spectroscopy[44,45] in Fig. 3. The electron chemical potentials needed are calculated in all cases within the LDA (Ref. 43) in order to study the effects of the GGA for positron states only. However, we have calculated that if the effect of the GGA (Ref. 38) on electron states is taken into account, the Fermi level raises and the magnitude of the positron affinity decreases by $\sim$ 0.3 eV. Compared to the LDA results the GGA for the positron states reduces the magnitude of the affinity by 0.3–0.7 eV due to the increase of the positron zero-point energy. The LDA is seen to overestimate the magnitude of the affinity within the $3d$ series and there the GGA is a clear improvement. In the case of the $4d$ and $5d$ transition metals studied the LDA results are, with the exception of Mo, in quite good agreement with experiments and the GGA leads to affinities with too small magnitudes in comparison with the experimental data. The trend that the GGA improves the LDA results for the $3d$ series while worsens them for the $4d$ and $5d$ series is also seen in

the case of electronic structure calculations for the cohesive properties such as the lattice constant and bulk moduli.[18]

B. Positron lifetimes at vacancies in solids

We have employed the present GGA model also in calculating annihilation characteristics for positrons trapped at ideal vacancies in solids. This means that the ions neighboring the vacancy are not allowed to relax from their ideal lattice positions. In the case of metal vacancies this is expected to be a good approximation because first-principles calculations indicate only very small relaxations.[49] For vacancies in semiconductors with more open lattice structures the ionic relaxations are more important (see, for example, Ref. 50 for the vacancy in Si and Refs. 51 and 52 for the vacancies in GaAs) and the relaxation may depend strongly on the charge state of the vacancy. In these cases the trapping of the positron has a tendency to compensate the inward relaxation of the vacancy.[53,52,7] Moreover, it has been shown that the charge state does not strongly affect the positron lifetime if the ionic relaxation is omitted.[54] As a result, the ideal (neutral) vacancy is a relevant reference system also in the case of semiconductors.

Another important issue for the calculations of positron states at vacancies is how the effects of the finite positron density on the electronic structure should be taken into account. As discussed in the Introduction, the conventional scheme used in the present calculations is a good starting point. To test this we performed a LDA two-component DFT (Ref. 6) calculation for a positron trapped at a vacancy in Cu. We used the LMTO ASA supercell method described below and the parametrization for the enhancement given in Ref. 7. The positron distribution obtained is close to and the positron lifetime is only about 2 ps shorter than that in the conventional LDA scheme. A similar agreement between the full two-component and the conventional scheme has been obtained previously for metal vacancies within the jellium model[6] and recently for the Ga vacancy in GaAs in a calculation using the pseudo-potential plane-wave description for electronic structure.[7] Encouraged by this experience, we will in this work compare the LDA and GGA models for the positron states by using only the computationally much more efficient conventional scheme.

In the vacancy calculations we use the supercell scheme, in which a large cell containing one vacancy is repeated periodically so that a regular superlattice of vacancies is formed. In order to get converged results for the positron lifetime, it is necessary to use such a large supercell that the positron wave function is vanishingly small at its boundaries when a vacancy is created at the center. In the atomic superposition calculations we have used supercells up to 255, 249, and 215 atoms for vacancies in fcc, bcc, and zinc-blende (or diamond) structures, respectively. In the LMTO ASA calculations the electronic structures of the vacancies are calculated using smaller super cells, which in the fcc, bcc, and zinc-blende structures contain 63, 63, and 31 atoms, respectively. In both methods the results are then extrapolated to the infinite supercell size. The slow convergence of the positron lifetime with the size of the supercell can be seen, for example, in the case of the vacancy in Cu. In the LMTO ASA calculations the converged lifetime is about 20 ps longer than that obtained with the small supercell of eight

B. BARBIELLINI *et al.*

TABLE II. Positrons trapped by vacancies in solids. The lifetimes τ and positron binding energies E_b are obtained with the LMTO ASA or the atomic superposition method using the LDA enhancement factor of Eq. (2) and the corresponding GGA with $\alpha = 0.22$.

		LMTO ASA				Atomic superposition			
Lattice	Material	τ^{LDA} (ps)	E_b (eV)	τ^{GGA} (ps)	E_b (eV)	τ^{LDA} (ps)	E_b (eV)	τ^{GGA} (ps)	E_b (eV)
fcc	Al	215	2.1	237	1.9	212	2.1	231	2.1
	Cu	158	1.7	193	1.9	153	1.3	200	1.5
bcc	Fe	159	2.6	186	2.7	158	3.4	183	3.7
	Nb	197	3.1	218	3.2	195	3.7	225	3.9
dia	Si	215	0.7	244	0.7	209	0.4	240	0.3
zb	GaAs, V_{Ga}					214	0.3	264	0.2
	GaAs, V_{As}					212	0.2	261	0.2

atomic sites. The atomic superposition method gives a similar trend with a positron lifetime increase of about 10 ps. We conclude that positron lifetimes obtained with supercells of four and eight atomic sites, which are used, for example, in the LMTO ASA calculations of Ref. 12, are not converged with respect to the positron distribution. This kind of supercell gives, however, reasonable estimates for positron lifetimes in comparison with experiments.

The results of our calculations for positron states at vacancies in solids are collected in Table II. For the vacancies in the diamond or zinc-blende structure the supercell calculations with the LMTO ASA method demand relatively more computer resources than the calculations for fcc and bcc metals, because empty spheres are needed. Therefore we have performed atomic superposition calculations in the case of vacancies in Si and GaAs and the LMTO ASA calculation only for the vacancy in Si. Within the LDA the LMTO-ASA method gives slightly longer positron lifetimes than the atomic superposition method. In the GGA the LMTO ASA lifetimes are either shorter or longer than the atomic superposition ones. The positron trapping energies are quite similar in both methods. The differences between the LMTO ASA and the atomic superposition results reflect the effects

of the self-consistency of the electronic density. As in the case of positron bulk lifetimes, these effects are more important in the GGA than in the LDA.

The theoretical positron lifetimes for vacancies are compared with experiment in Table III. The first column gives the experimental lifetimes for positrons trapped at different vacancies. For the experiment-theory comparison the ratios between the vacancy and bulk lifetimes are calculated from the experimental works and from the results of Tables I and II. It can be seen that within the calculation scheme, LMTO ASA, or atomic superposition, the LDA and the GGA models give similar ratios. For the metal vacancies the lifetime ratios obtained using the atomic superposition method are of the same order as or slightly smaller than the experimental ones. The ratios from the LMTO ASA calculations are systematically larger than those from the atomic superposition method, reflecting a stronger localization of the positron at the vacancy. The reason for the differences between the LMTO ASA and the atomic superposition methods can be understood as follows. In the former self-consistent calculation a dipole-type potential arises so that electron density is transferred from the vacancy region (the vacancy sphere and its 12 nearest-neighbor atomic spheres) further away to the

TABLE III. Positrons trapped by vacancies in solids. The experimental positron lifetimes τ_{expt}^{vac} are given. The ratios between the vacancy and bulk lifetimes are calculated from the experimental results (Expt.) and from the theoretical results obtained with the LMTO ASA or the atomic superposition method using the LDA enhancement factor of Eq. (2) and the corresponding GGA with $\alpha = 0.22$.

		τ^{vac}/τ^{bulk}					
			LMTO ASA		Atomic superposition		
Material	τ_{expt}^{vac} (ps)	Expt.	LDA	GGA	LDA	GGA	
Al	251 [a]	1.54 [a]	1.49	1.55	1.42	1.44	
Cu	179 [b]	1.63 [b]	1.65	1.64	1.51	1.54	
Fe	175 [c]	1.59 [c]	1.75	1.72	1.68	1.65	
Nb	210 [d]	1.72 [d]	1.81	1.79	1.71	1.67	
Si			1.16	1.16	1.14	1.16	
GaAs, V_{Ga}^{3-}	260 [e]	1.13 [e]			1.13	1.14	
GaAs, V_{As}^{-}	257 [f]	1.11 [f]			1.12	1.13	
GaAs, V_{As}^{0}	295 [f]	1.28 [f]					

[a]From Ref. 55.
[b]From Ref. 56
[c]From Ref. 57.

[d]From Ref. 58.
[e]From Ref. 59.
[f]From Ref. 60.

region of the perfect lattice. The dipole, reversed for the positron potential, results in a localization of the positron wave function that is stronger than in the atomic superposition calculations. This strong positron localization increases the positron lifetime. Note that the feedback effect discussed above in the context of the bulk lifetimes is not effective for this kind of longe-range field.

The vacancy-bulk lifetime ratios obtained with the LMTO ASA and the atomic superposition method for Si are very similar. The experimental vacancy-bulk lifetime ratios for the triply negative Ga vacancy and the singly negative As in GaAs agree well with the atomic superposition results for the ideal vacancies. The much larger experimental ratio for the neutral As vacancy may be a result of a large lattice relaxation occurring between the negative and the neutral charge states.[51]

C. Angular correlation of annihilation radiation

1. 2D ACAR spectra

The 2D ACAR technique stands out in its unique capability to yield high-resolution information about the momentum density and the Fermi surface (FS) of metals. Moreover, the LCW theorem[33] proposes that when the 2D ACAR spectrum is folded into the first Brillouin zone, mainly the structures related to the FS remain. In some cases, the FS breaks can be inferred just by studying the occupation of the bands crossing the Fermi energy. However, the presence of the positron makes the procedure inexact, because the background is modulated by positron annihilation with the electronic states that do not contribute to the FS. These positron wave function effects are included within the IPM. However, again enhancement has to be considered, although it is not of such crucial importance as in describing the positron lifetime.

For example, in the case of Cu a careful comparison of the 2D ACAR distributions shows a considerable deviation between the IPM and the experiment.[63,64] The deviation is attributed to many-body effects. In order to compare theory with experiment, Wakoh *et al.*[63] considered the ratio

$$r(p_x,p_y) = \frac{N^{\text{expt}}(p_x,p_y) - N^{\text{IPM}}(p_x,p_y)}{N^{\text{IPM}}(p_x,p_y)}, \quad (18)$$

where N^{expt} and N^{IPM} are normalized to the same volume. The shape of $r(p_x,p_y)$ indicates that the many-body enhancement increases as the first Brillouin zone is approached; outside this zone the enhancement gradually diminished, indicating that for tightly bound electrons the enhancement is smaller than for the sp conduction electrons in the first zone. We have performed a detailed study on copper to check whether the LDA and the GGA explain these trends.

The momentum density of annihilating positron-electron pairs for the valence states in Cu is shown in Fig. 4(a) along the direction Γ-X (at the X point, $p \approx 6.7$ mrad). Due to a symmetry-induced selection rule,[65] only two bands, which are hybridizations of an sp-like and a d-like conduction band, contribute along this direction. The FS breaks are clearly visible within the first and second Brillouin zones. These discontinuities are not shifted by the electron-positron correlation, which is in agreement with the Majumdar
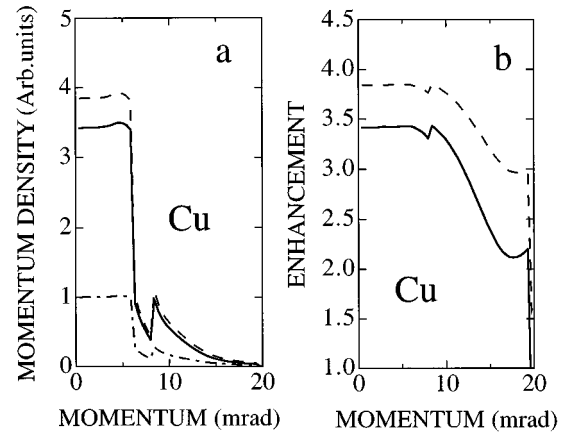

FIG. 4. (a) Momentum density and (b) the corresponding enhancement factor for annihilating positron-electron pairs for Cu along the direction Γ-X in the momentum space. The densities are normalized to give the relative total valence annihilation rates. The solid, dashed, and dash-dotted lines are the results in the GGA, LDA, and IPM calculations, respectively.

theorem.[66] At low momenta mainly the sp bands contribute. The relative contribution of the localized d electrons increases towards higher Brillouin zones with the maximum around $11-13$ mrad. Wakoh *et al.*[63] concluded that the IPM overestimates the contributions of the d electrons. Figure 4(b) shows that both the LDA and the GGA predict a reduction of the enhancement in the momentum region where the d electrons dominate and should improve the theoretical fit to the experimental data.

In order to find out whether the LDA or the GGA agrees better with the experiment, we have compared the shapes of the 2D ACAR distributions in Fig. 5. The figure shows the calculated 2D ACAR spectra containing the contributions from both the core and valence electrons and corresponding to the momentum distribution (4) integrated in the [111] direction. The corresponding experimental data[64] are also shown. A cut of the two-dimensional map along the [1–1 0]

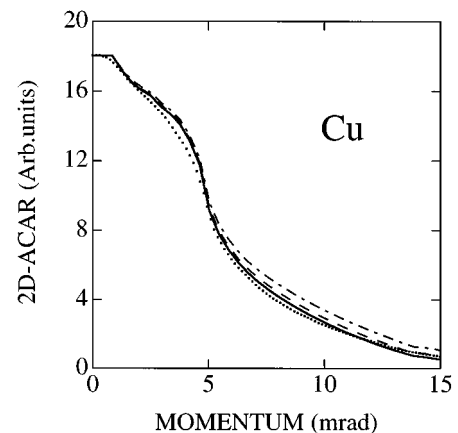FIG. 5. Two-dimensional ACAR spectra for Cu. The momentum densities are integrated in the [111] direction and normalized to the same value at the zero momentum. The cuts along the [1−10] direction are given. The solid, dashed, and dash-dotted lines are the results in the GGA, LDA, and IPM calculations, respectively. The experimental points are given by dots.
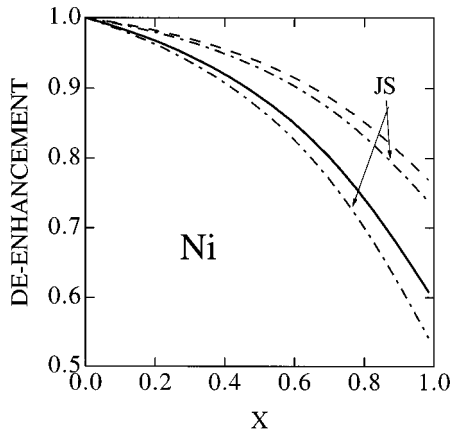
B. BARBIELLINI *et al.*

FIG. 6. Deenhancement for the Ni d electrons as a function of the relative position of the energy eigenvalue within the d bands. For the definitions, see the text. The solid and dashed lines give the GGA and LDA results, respectively. The upper and lower dash-dotted lines are the result of the Jarlborg-Singh theory with $\mu = 1/2$ and 1, respectively (Ref. 68).

direction is given. The effect of the enhancement factor is to favor annihilation in the interstitial, low-electron-density regions of the lattice and the gradient correction makes this trend stronger. As a result, the localization of annihilation in the momentum space increases from the IPM to the LDA and further to the GGA. The suppression is important in the region around 10 mrad, where the contribution of the d electrons dominates. On the basis of Fig. 5 one can conclude that these trends improve the agreement with experiment.

2. Deenhancement of d-electron annihilation

Two dimensional ACAR studies for the transition metals indicate that the enhancement factor for the d electrons is clearly smaller than that for the s and p electrons.[3,13] Jarlborg and Singh[61] have shown that the LDA approach for the electron-positron enhancement can account for the observed trends. The enhancement factor they use is obtained by solving a two-body problem for a positron and an electron in a correlation cell of radius r_s determined by the local electron density. In the original model, the reduced mass μ of the electron-positron pair is treated as a free parameter and the comparison with the experimental 2D ACAR results does not give a unique value for μ. The positron lifetime calculations[62] show unambiguously that the correct value is $\mu = 1/2$. However, in some cases, e.g., for Ni, the theoretical 2D ACAR results calculated with the value of $\mu = 1$ agree clearly better with experiment than those calculated with the value of $\mu = 1/2$. This fact indicates that the actual enhancement should be more delocalized within the Wigner-Seitz cell than that calculated with $\mu = 1/2$. Below we show that this apparent contradiction is solved within our GGA scheme for the positron annihilation.

It has been suggested that the enhancement depends on the electronic binding energy.[67,68] Figure 6 gives the so-called deenhancement for the Ni d electrons[68,61] as a function of the energy eigenvalue E. Actually, the abscissa is the relative position $x = (E - E_{bot})/(E_F - E_{bot})$ within the d bands. Above, E_F denotes the Fermi energy and E_{bot} the

bottom of the energy band at the Γ point. The deenhancement is defined as the enhancement at the energy in question divided by the enhancement at the bottom of the d bands. In practice, we calculate the enhancement factor for a given energy by integrating over the Wigner-Seitz sphere the local enhancement factor weighted by the positron density and the density of the LMTO ASA partial wave at that energy. Figure 6 shows that the enhancement is stronger for the relatively more delocalized bonding states at the bottom of the d band than for the more localized antibonding states at the top of the d band. The GGA increases the sensitivity of the enhancement factor to the d electron localization and the related energy eigenvalue. Jarlborg and Singh[61] showed that they could fit well the experimental LCW in Ni using their enhancement with $\mu = 1$. However, the use of $\mu = 1$ gives a wrong value for the lifetime.[62] Figure 6 shows that the GGA gives a similar deenhancement. In conclusion, the GGA gives a lifetime value and momentum distribution in good agreement with the experiments.

It should be noted that the approximation of averaging the enhancement factor over the electronic states cannot describe the increase of the enhancement for the nearly free sp electrons close to the Fermi momentum as it is predicted in the Kahana theory.[29] Daniuk *et al.*[28] have proposed a method that treats the enhancement corrections locally in real space using the jellium approximation. This method predicts both the relative deenhancement for the d electrons and the increase of the enhancement as a function of the increasing electron energy for the nearly electron-gas systems. A straightforward gradient correction for the scheme of Daniuk *et al.* can be obtained by using a formulation similar to Eq. (13).

According to the above theoretical model, the deenhancement for the d electrons close to the Fermi level is most pronounced for metals with filled d band. Examples are Ni and Pd. This is in good agreement with experimental results.[13] In the early transition metals the Fermi level lies below the center of the d bands. Therefore, it is expected that the influence of the enhancement for the momentum distribution of the annihilating positron-electron pairs is smaller than for the late transition metals and that already the IPM produces good results. Indeed, the LCW-folded experimental data for V and Nb reflect well the electron momentum distribution in the first Brillouin zone, i.e., the LCW theorem is fairly well fulfilled. Nevertheless, in order to obtain good agreement between theory and experiment for the relative strength of the core contribution, it is necessary to use the enhancement factor, which accounts for the smaller enhancement of the localized core states relative to the valence states.

3. Fermi surface study in high-temperature superconductors

Since the advent of high-temperature superconductivity in the copper oxides, it was felt that strong electron correlation effects must be involved. While searching for the FS, it is natural to wonder which is the influence of the strong correlations on the electronic structure. Actually the nature and the existence of the FS is the crucial point in many theories of the superconductivity.[69] The relative mastery in calculating the positron-electron correlation effects in lifetime and in 2D ACAR with the methods outlined above encourages us to
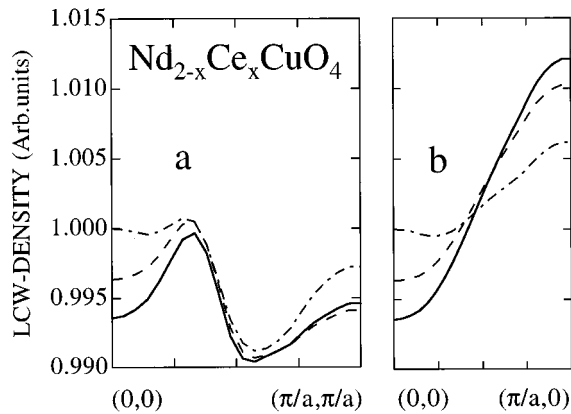
FIG. 7. LCW-folded calculated 2D ACAR spectra for $Nd_{2-x}Ce_xCuO_4$. The momentum densities are integrated along the direction of the c axis of the body-centered tetragonal lattice and normalized to the same volume. The cuts along the direction (a) of the diagonal of the ab plane as well as (b) along the a axis are given. The solid, dashed, and dash-dotted lines are the results in the GGA, LDA, and IPM, respectively.

make theoretical predictions on the FS signal arising in positron annihilation measurements. Moreover, the large charge-density inhomogeneities in the high-temperature superconductors suggest that the GGA should have, in comparison to the LDA, a strong effect on the positron annihilation in these materials.

With respect to the 2D ACAR measurements, the situation in copper oxides differs sharply from that in simple metals, in which the FS effects dominate. In copper oxides the spatial distribution of the positron wave function has a large influence on the ACAR maps, whereas the FS signals are weak. Actually a combined experimental and theoretical study[70] for $La_{2-x}Ce_xCuO_4$ reveals strong effects due to the positron-electron overlap in experimental data, consistent with the theoretical calculations. The authors also found discontinuities in the LCW folding from Sr-doped sample consistent with the presence of a FS.

$Nd_{2-x}Ce_xCuO_{4-\delta}$ is a good candidate for probing the Fermi surface. This is because the positron density has a substantial overlap with the Cu-O planes. The LCW-folded 2D ACAR spectra for $Nd_{2-x}Ce_xCuO_{4-\delta}$ calculated within the IPM, LDA, and GGA are shown in Fig. 7. The Fermi surface breaks in the direction shown are already modulated by the wave-function effects in the IPM. The effects of tak-

ing into account the enhancement are similar to that of the positron wave function and consequently the relative signal at the low-density regions strengthens when the enhancement is included. The GGA is more sensitive to the electronic structure than the LDA. Therefore, as shown in Fig. 7, the partial annihilation rates vary more and the LCW spectrum is more modulated in the GGA than in the LDA. As a matter of fact, a recent 2D ACAR experiment for $Nd_{2-x}Ce_xCuO_{4-\delta}$ (Ref. 71) indicates a Fermi surface signal in good agreement with a calculation based on the present GGA scheme.[72] However, as the real sample contains some defects, we cannot extract unambiguously the experimental correlations effects to compare with the theory. Nevertheless, our calculation predicts that the GGA electron-positron correlation makes the LCW more modulated, but does not spoil the possibility to observe the FS in $Nd_{2-x}Ce_xCuO_{4-\delta}$.

IV. CONCLUSION

We have made a comprehensive study of the recently introduced gradient correction scheme for positron states and annihilation in several types of solids. We have considered positron lifetimes in perfect crystal lattices as well as trapped by vacancy defects. The positron energetics is monitored by calculating the positron affinities. Moreover, we have studied the effects of the gradient correction on the momentum distribution of the annihilating positron-electron pairs using several representations. The gradient correction improves systematically the too large annihilation rates obtained in the LDA and generally brings them into good agreement with existing experimental positron lifetimes. The GGA gives also a natural explanation for the so-called deenhancement for the annihilation of the d electrons discussed in the context of the 2D ACAR maps of certain transition metals.

The GGA approach is more sensitive to the quantum-mechanical shell structure and to the self-consistency of the electron density than the LDA. This calls for the use of the most sophisticated self-consistent electronic-structure calculation methods. On the other hand, this means that positron measurements contain more detailed electronic-structure information than has been previously thought and the GGA can open a way for extracting it.

[1] *Positron Solid State Physics*, edited by W. Brandt and A. Dupasquier (North-Holland, Amsterdam, 1983).

[2] P. J. Schultz and K. G. Lynn, Rev. Mod. Phys. **60**, 701 (1988).

[3] S. Berko, in *Momentum Distributions*, edited by R. N. Silver and P. E. Sokol (Plenum, New York, 1989), p. 273.

[4] M. J. Puska and R. M. Nieminen, Rev. Mod. Phys. **66**, 841 (1994).

[5] R. O. Jones and O. Gunnarsson, Rev. Mod. Phys. **61**, 689 (1989).

[6] E. Boroński and R. M. Nieminen, Phys. Rev. B **34**, 3820 (1986).

[7] M. J. Puska, A. P. Seitsonen, and R. M. Nieminen, Phys. Rev. B **52**, 10 947 (1995).

[8] M. Šob, in Positron Annihilation, edited by Yuan-Jin He, Bi-Song Cao, and Y.C. Jean [Mater. Sci. Forum **175-178**, 855 (1995)].

[9] K. O. Jensen and A. B. Walker, J. Phys. F **18**, L277 (1988).

[10] M. J. Puska and R. M. Nieminen, Phys. Rev. B **46**, 1278 (1992).

[11] K. O. Jensen, J. Phys. Condens. Matter **1**, 10 595 (1989).

[12] P. A. Sterne and J. H. Kaiser, Phys. Rev. B **43**, 13 892 (1991).

[13] P. Genoud, Ph.D. thesis, Geneva University, 1990; A.A. Manuel, A.K. Singh, T. Jarlborg, P. Genoud, L. Hoffmann, and M. Peter, in *Positron Annihilation*, edited by L. Dorikens, *et al.* (World-Scientific, Singapore, 1989), p. 833.

[14] H. Stachowiak and J. Lach, Phys. Rev. B **48**, 9828 (1993).

[15] W. E. Pickett, Comments Solid State Phys. **12**, 1 (1985).

[16] J. P. Perdew, Physica B **172**, 1 (1991).

[17] P. Bagno, O. Jepsen, and O. Gunnarsson, Phys. Rev. B **40**, 1997 (1989).

[18] B. Barbiellini, E. G. Moroni, and T. Jarlborg, J. Phys. Condens. Matter **2**, 7597 (1990); Helv. Phys. Acta **64**, 164 (1991).

[19] B. Hammer, M. Scheffler, K. W. Jacobsen, and J. K. Nórskov, Phys. Rev. Lett. **73**, 1400 (1994); J. A. White, D. M. Bird, M. C. Payne, and I. Stich, *ibid.* **73**, 1404 (1994).

[20] G. Ortiz and P. Ballone, Phys. Rev. B **43**, 6376 (1991).

[21] J. P. Perdew, J. A. Chevary, S. H. Vosko, K. A. Jackson, M. R. Pederson, D. J. Singh, and C. Fiolhais, Phys. Rev. B **46**, 6671 (1992); **48**, 4978(E) (1993).

[22] B. Barbiellini, M. J. Puska, T. Torsti, and R. M. Nieminen, Phys. Rev. B **51**, 7341 (1995).

[23] J. Arponen and E. Pajanne, Ann. Phys. (N.Y.) **121**, 343 (1979); in *Positron Annihilation*, edited by P. C. Jain, R. M. Singru, and K. P. Gopinathan (World Scientific, Singapore, 1985), p. 21.

[24] A. Kheim, D. J. Singh, and C. J. Umrigar, Phys. Rev. B **51**, 4105 (1995).

[25] Y. M. Juan, E. Kaxiras, and R. G. Gordon, Phys. Rev. B **51**, 9521 (1995).

[26] O. K. Andersen, O. Jepsen, and M. Šob, in *Electronic Band Structure and Its Applications*, edited by M. Yussouff (Springer-Verlag, Heidelberg, 1987), p. 1.

[27] M. J. Puska and R. M. Nieminen, J. Phys. F **13**, 333 (1983).

[28] S. Daniuk, G. Kontrym-Sznajd, J. Majers, A. Rubaszek, H. Stachowiak, P. A. Walters, and R. N. West, in *Positron Annihilation* (Ref. 23), pp. 43 and 279; J. Phys. F **17**, 1365 (1987); S. Daniuk, J. Phys. Condens. Matter **1**, 5561 (1989).

[29] S. Kahana, Phys. Rev. **129**, 1622 (1963).

[30] A. P. Seitsonen, M. J. Puska, and R. M. Nieminen, Phys. Rev. B **51**, 14 057 (1995).

[31] L. Oberli, Ph.D. thesis, Geneva University, 1985; L. Oberli, A. A. Manuel, R. Sachot, P. Descout, M. Peter, L. P. L. Rabou, P. E. Mijnarends, T. Hyodo, and A. T. Stewart, Phys. Rev. B **31**, 1147 (1985).

[32] A. Rubaszek, Phys. Rev. B **44**, 10857 (1991); J. Phys. Condens. Matter **1**, 2141 (1989).

[33] D. G. Lock, V. H. C. Crisp, and R. N. West, J. Phys. F **3**, 561 (1973).

[34] L. Lantto, Phys. Rev. B **36**, 5160 (1987).

[35] D. M. Ceperley and B. J. Alder, Phys. Rev. Lett. **45**, 566 (1980).

[36] G. Ortiz, Ph.D. thesis, Ecole Polytechnique Fédérale de Lausanne, 1992.

[37] C. H. Leung, M. J. Stott, and C. O. Almbladh, Phys. Lett. **57A**, 26 (1976).

[38] J. P. Perdew, in *Electronic Structure of Solids '91*, edited by P. Ziesche and H. Eschrig (Akademie-Verlag, Berlin, 1991).

[39] B. Barbiellini, Phys. Lett. A **134**, 328 (1989).

[40] T. Chiba, G. B. Dürr, and W. Brandt, Phys. Status Solidi B **81**, 609 (1977).

[41] M. J. Puska, M. Mäkinen, M. Manninen, and R. M. Nieminen, Phys. Rev. B **39** 7666 (1989).

[42] R. M. Nieminen and C. H. Hodges, Solid State Commun. **18** 1115 (1976).

[43] M. J. Puska, P. Lanki, and R. M. Nieminen, J. Phys. Condens. Matter **1**, 6081 (1989).

[44] M. Jibaly, A. Weiss, A. R. Koymen, D. Mehl, L. Stiborek, and C. Lei, Phys. Rev. B **44**, 12 166 (1991).

[45] D. W. Gidley and W. E. Frieze, Phys. Rev. Lett. **60**, 1193 (1988).

[46] A. K. Singh and T. Jarlborg, J. Phys. F **15**, 727 (1985).

[47] S. Daniuk, M. Šob, and A. Rubaszek, Phys. Rev. B **43**, 2580 (1991).

[48] The experimental positron bulk lifetimes used are from the following sources: Na (338 ps) and K (397 ps) by H. Weisberg and S. Berko, Phys. Rev. **154**, 249 (1967); Al (170 ps), Fe (112 ps), Ni (107 ps), Cu (120 ps), Si (216 ps), Ge (228 ps), GaAs (231 ps), and InP (244 ps) by K. Saarinen (unpublished); CdTe (285 ps) by C. Gély-Sykes, C. Corbel, and R. Triboulet, Solid State Commun. **80**, 79 (1993).

[49] M. J. Mehl and B. M. Klein, Physica B **172**, 211 (1992); R. Benedek, L.H. Yang, C. Woodward, and B. I. Min, Phys. Rev. B **45**, 2607 (1992).

[50] O. Sugino and A. Oshiyama, Phys. Rev. Lett. **68**, 1858 (1992).

[51] K. Laasonen, M. J. Puska, and R. M. Nieminen, Phys. Rev. B **45**, 4122 (1992).

[52] L. Gilgien, G. Galli, F. Gygi, and R. Car Phys. Rev. Lett. **72**, 3214 (1994).

[53] K. Laasonen, M. Alatalo, M. J. Puska, and R. M. Nieminen, J. Phys. Condens. Matter **3**, 7217 (1991).

[54] M. J. Puska, O. Jepsen, O. Gunnarson, and R. M. Nieminen, Phys. Rev. B **34**, 2695 (1986); M. Alatalo, M. J. Puska, and R. M. Nieminen, J. Phys. Condens. Matter **5**, L307 (1993).

[55] H. E. Schaefer, R. Gugelmeier, M. Schmolz, and A. Seeger, in *Proceedings of the Vth Risó International Symposium of Metallurgy and Materials Science*, edited by N. H. Andersen, M. Eldrup, N. Hansen, D. J. Jensen, T. Leffers, H. Lillholt, O. B. Pedersen, and B. N. Singh (Risó National Laboratory, Risó, 1984).

[56] H. E. Schaefer, W. Stuck, F. Banhart, and W. Bauer, in *Proceedings of the 8th International Conference on Vacancies and Interstitials in Metals and Alloys,* edited by C. Ambromeit and H. Wollenberger (Trans Tech, Aedermannsdorf, 1986).

[57] A. Vehanen, P. Hautojärvi, J. Johansson, and J. Yli-Kauppila, Phys. Rev. B **25**, 762 (1982).

[58] P. Hautojärvi, H. Huomo, M. Puska, and A. Vehanen, Phys. Rev. B **32**, 4326 (1985).

[59] C. Corbel, F. Pierre, K. Saarinen, P. Hautojärvi, and P. Moser, Phys. Rev. B **41**, 10 632 (1990); **45**, 3386 (1992).

[60] K. Saarinen, P. Hautojärvi, P. Lanki, and C. Corbel, Phys. Rev. B **44**, 10 585 (1991).

[61] T. Jarlborg and A.K. Singh, Phys. Rev. B **36**, 4660 (1987).

[62] B. Barbiellini, P. Genoud, and T. Jarlborg, J. Phys. Condens. Matter **3**, 7631 (1991).

[63] S. Wakoh, S. Berko, M. Haghgooie, and J. J. Mader, J. Phys. F **9**, L231 (1979).

[64] A. A. Manuel, S. Samoilov, Ø. Fischer, and M. Peter, Helv. Phys. Acta **52**, 255 (1979).

[65] R. Harthoorn and P. E. Mijnarends, J. Phys. F **8**, 1147 (1978).

[66] C. K. Majumdar, Phys. Rev. **140**, A227 (1965).

[67] M. Šob, in *Proceedings of the 8th Annual International Symposium on Electronic Structure of Metals and Alloys, Gaussig*, edited by P. Ziesche (Tech. Universität, Dresden 1978), p. 170; J. Phys. F **12**, 571 (1982); P. E. Mijnarends and R. M. Singru, Phys. Rev. B **19**, 6038 (1979).

[68] A. K. Singh, A. A. Manuel, T. Jarlborg, Y. Mathys, E. Walker, and M. Peter, Helv. Phys. Acta **59**, 410 (1986).

[69] M. Weger, B. Barbiellini, and M. Peter, Z. Phys. B **94**, 387 (1994).

[70] P. A. Sterne, R. H. Howell, M. J. Fluss, J. H. Kaiser, K. Ki-

tazawa, and H. Kojima, J. Phys. Chem. Solids **54**, 1231 (1993); R. H. Howell, P. A. Sterne, M. J. Fluss, J. H. Kaiser, K. Kitazawa, and H. Kojima, Phys. Rev. B **49**, 13 127 (1994).

[71] A. A. Manuel, A. Shukla, L. Hoffmann, T. Jarlborg, B. Barbiellini, S. Massidda, W. Sadowski, E. Walker, A. Erb, and M.

Peter, J. Phys. Chem. Solids **56**, 1951 (1995); A. Shukla, B. Barbiellini, L. Hoffmann, A. A. Manuel, W. Sadowski, E. Walker, and M. Peter, Phys. Rev. B **53**, 3613 (1996).

[72] B. Barbiellini, M. J. Puska, A. Harju, and R. M. Nieminen, J. Phys. Chem. Solids **56**, 1693 (1995).